π-plasmon dispersion in free-standing graphene by momentum-resolved electron energy-loss spectroscopy

S. C. Liou,[1,2] C.-S. Shie,[3] C. H. Chen,[1] R. Breitwieser,[1] W. W. Pai,[1] G. Y. Guo,[3,*] and M.-W. Chu[1,4,†]

[1]*Center for Condensed Matter Sciences, National Taiwan University, Taipei 10617, Taiwan*

[2]*Maryland NanoCenter, University of Maryland, College Park, Maryland 20742, USA*

[3]*Department of Physics, National Taiwan University, Taipei 10617, Taiwan*

[4]*Taiwan Consortium of Emergent Crystalline Materials, Ministry of Science and Technology, Taipei 10617, Taiwan*

The π-plasmon dispersion in graphene was scrutinized by momentum-resolved electron energy-loss spectroscopy with an improved momentum q resolution and was found to display the square root of the q dispersion characteristic of the collective excitation of two-dimensional electron systems, in contrast to previous experimental and theoretical studies which reported a linear q dispersion. Our theoretical elaborations on the q-dependent spectra affirm this square root of q relation and further unveil an in-plane electronic anisotropy. The physical property of the π plasmon is thoroughly compared to that of the two-dimensional plasmon due to carriers of the Dirac fermions. A clear distinction between the π plasmon and the two-dimensional Dirac plasmon is demonstrated, clarifying the common notion about correlating the linearly dispersed Dirac cones with the linear dispersion of the π plasmon previously reported.

I. INTRODUCTION

Graphene, a single layer of carbon atoms densely packed in a honeycomb lattice, is the first stable two-dimensional (2D) material found in the atmosphere [1,2]. This 2D carbon sheet comprises a conical-band character of Dirac fermions at the corners of Brillouin zone (BZ) showing a distinct linear q dependence [1–3], and graphene continues to be the model system in the search for emergent 2D phenomena, ranging from topological states to anomalies in monolayer transition-metal dichalcogenides [4,5].

In graphene, the 2D Dirac fermions are massless and exhibit remarkably high, robust carrier mobility upon temperature variations [1–3.] These features add a plethora of novel device applications [1], in analogy with a 2D electron gas (2DEG) in conventional semiconductor heterojunctions. Using q-dependent electron energy-loss spectroscopy (EELS), the collective plasmon excitation of the 2D electrons (with density generally of the order of $\sim 10^{13}$ cm^{-2}) is found to form an otherwise dispersive feature at 0–1 eV, with the characteristic $\sqrt{q}$ dependence being distinctly different from the linearly dispersed Dirac cones of a single-particle characteristic [3,6–12]. This $\sqrt{q}$ dispersion has been theoretically investigated in detail and has been demonstrated to be the signature of collective quasiparticle excitations with a 2D nature [3,6–9]. Such a 2D Dirac plasmon with its low excitation energy boasts another intriguing characteristic of graphene, plasmonics applications in the near- and far-infrared regimes [10,11]. Indeed, the technological merit of graphene continues to grow with the increasing understanding of the Dirac fermions [1,2,12]. Apart from these intriguing characteristics, the elementary structure of graphene is nonetheless determined by the π and σ valence electrons lying outside the Dirac cones, with the former being unpaired in an out-of-plane orbital and the latter being

hybridized with the three coordinated carbons in the ab plane, like in parent graphite [1–3,13,14].

In graphene and also parent graphite, the π and σ electrons manifest the related collective excitations of π and $\pi + \sigma$ plasmons above ~ 4 and ~ 15 eV, respectively [15–22]. Moreover, both the collective excitations of parent graphite show a quadratic dispersion (proportional to q^2) in line with the typical dynamical response in three-dimensional (3D) bulks [3,20–22]. By contrast, graphene is a perfectly 2D matter, and its collective π and $\pi + \sigma$ plasmons oscillate in the 2D plane, intuitively giving rise to a 2D character of the plasmons, just like the 2D Dirac plasmon at 0–1 eV [3,6–9]. Surprisingly, three recent q-dependent EELS studies of the π plasmon of graphene reported a quasilinear dispersion [17–19], which is a general characteristic of the plasmon excitations of one-dimensional electron systems [3,16], and a separate theoretical work on the subject also pointed out the same dispersion feature [23]. These works represent the detailed works on the π-plasmon dispersions of graphene [17–19,23], while the linear dispersion derived is at odds with the established notion of the $\sqrt{q}$-dispersion characteristic of 2D systems [3,6–9]. An elaborate q-dependent EELS investigation, which has largely escaped experimental scrutiny due to the focus on the 2D Dirac plasmon [3,6–11], is essential for shedding light on this inconsistency.

In this work, we report q-dependent EELS studies of the π plasmon in free-standing graphene with an improved q resolution of ~ 0.001 Å^{-1} over the entire BZ and a momentum transfer up to the zone boundary of ~ 1.5 Å^{-1}. The previous q-dependent EELS studies showed a q resolution of the order of ~ 0.01 Å^{-1} and/or accessed only a fraction of the BZ [6–8,16–19]. With the fine q resolution and extensive q range, we were able to explore the π plasmon along the two principal in-plane directions, $\bar{\Gamma}\bar{M}$ and $\bar{\Gamma}\bar{K}$, at high precision and consistently found the $\sqrt{q}$-dispersion characteristic of 2D collective excitations. A further tilting experiment with graphene, allowing out-of-plane contributions to the EELS

―――――――
*Corresponding author: gyguo@phys.ntu.edu.tw

†Corresponding author: chumingwen@ntu.edu.tw

excitation, indicated that the π-plasmon dispersion is free from any out-of-plane dispersive component, unveiling the true 2D character of the π plasmon without ambiguity [3,4,6–9]. The EELS results along with an in-plane electronic anisotropy observed at large q are theoretically investigated, and the dispersion of the $\pi + \sigma$ plasmon is also discussed.

II. EXPERIMENTS AND THEORETICAL CALCULATIONS

The EELS experiments were performed on a transmission electron microscope (TEM; FEI Tecnai F20), operated at 120 kV and equipped with a field-emission gun. To achieve the superb q resolution required for resolving the π-plasmon dispersion of graphene unambiguously, an exceptionally long camera length of the diffraction pattern is crucial, and this can be attained by raising the sample-object plane so as to use the graphene as an optical grating of the incident parallel illumination by itself (detailed methodology is given in Ref. [24]), resulting in a camera length of ∼92 m. Using an EELS slit size of 4×10^{-4} m and a finite diffraction spot focused on the slit, a q resolution of ∼0.001 Å^{-1} was derived. The accompanying EELS energy resolution is ∼0.6 eV.

The graphene sheet was grown on a Cu foil by chemical vapor deposition and was then transferred onto a TEM grid in a free-standing form. Careful monitoring of the diffraction-spot intensity revealed the monolayer feature in many patches (a few tens of micrometers in the lateral dimension) of the thus-prepared sample [25], and the EELS results were acquired from these regions. The EELS experiments with graphite were conducted on exfoliated natural graphite with a thickness of ∼40 nm.

The theoretical understanding of our EELS observations was undertaken in the framework of the density functional theory with the local-density approximation (LDA) plus the linear response of the random-phase approximation (RPA) and otherwise adiabatic LDA (ALDA) [26,27]. We use the accurate real-space projector augmented-wave function (PAW) [28], which is implemented in the GPAW code [29]. Graphene is simulated by a slab supercell with the in-plane lattice constant a of 2.46 Å and an elevated interlayer spacing of 25 Å in order to assure a good convergence. A grid spacing of 0.2 Å was used throughout all calculations. In addition, a k sampling with 25 $\times$ 25 $\times$ 1 for the 2D BZ was exploited in the self-consistent calculation of the band structure. A denser k-point mesh of 100 $\times$ 100 $\times$ 1 and a plane-wave energy cutoff up to 200 eV (i.e., including 819 plane waves) were taken into account upon the evaluation of the theoretical q-dependent EELS spectra, which further integrate the 50 bands up to 40 eV above the Fermi level. For comparison, we have also performed the same calculations for graphite. The lattice constants $a = 2.46$ Å and $c = 6.71$ Å were used. A k-sampling mesh of 20 $\times$ 20 $\times$ 7 was used in the self-consistent band structure calculation, and a fine k-point mesh of 40 $\times$ 40 $\times$ 14 was used in the calculation of the q-dependent dielectric function and EELS spectra.

III. RESULTS AND DISCUSSION

The q-resolved EELS experiments of graphene were performed along both $\bar{\Gamma}\bar{M}$ and $\bar{\Gamma}\bar{K}$. In Fig. 1(a) along $\bar{\Gamma}\bar{M}$, the superb q resolution facilitates a direct observation of the
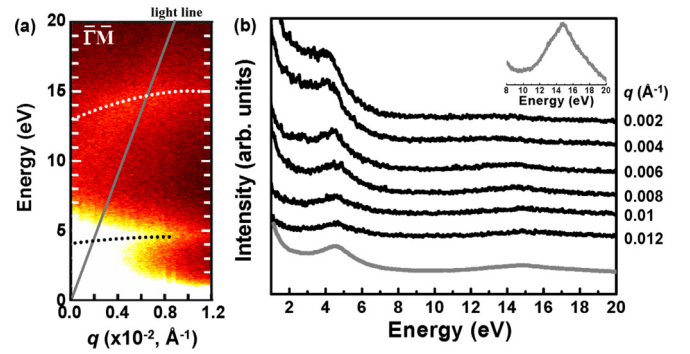

FIG. 1. (Color online) (a) The q-dependent EELS map in the long-wavelength limit of graphene along $\bar{\Gamma}\bar{M}$. The gray line is the light line. The curved dashed lines are guides for the eyes for the characteristic nonlinear dispersions derived from the peak positions revealed in (b). (b) The EELS spectra extracted from (a) at the indicated q. The bottom gray line shows the EELS spectrum integrated over the whole q range of $0 - 0.012$ Å^{-1} in (a). The inset shows a close-up of the $\pi + \sigma$-plasmon portion of the gray spectrum.

dispersive π and $\pi + \sigma$ plasmons in the long-wavelength limit, starting from ∼4 and ∼13 eV at $q \rightarrow 0$, respectively. The dispersive feature of these excitations in such a small q range $(0 - 0.012$ Å$^{-1})$ has never been resolved due to a compromised q resolution of the previous reports $(0.03 - 0.06$ Å$^{-1})$ [17–19]. Although the strong elastic peak tends to saturate the intensity of Fig. 1(a) below ∼3 eV, both plasmons point to a nonlinear dispersion, which will be affirmed in Figs. 2 and 3. In Fig. 1(b), we show the EELS spectra extracted from Fig. 1(a) with $q \approx 0.002 - 0.012$ Å^{-1}. The integrated spectrum over the whole q range is also exhibited [bottom gray curve in Fig. 1(b)], and the thus-indicated π- and $\pi + \sigma$-plasmon peaks at ∼4.5 and ∼15 eV (also see the inset), respectively, are consistent with the well-known excitation energies resolved by scanning TEM (STEM) that typically integrate over q as a result of the convergent-beam optics [15]. This agreement with the STEM results reaffirms the benefit and necessity of performing EELS experiments with high q resolution under these circumstances, and with this reinforced confidence level of our q-resolved setup, we now proceed to the dispersion over the whole BZ along $\bar{\Gamma}\bar{M}$ and $\bar{\Gamma}\bar{K}$ (Fig. 2).

Figures 2(a) and 2(b) show the large-q dispersion along $\bar{\Gamma}\bar{M}$ up to the BZ boundary (∼1.5 Å^{-1}) and the EELS spectra acquired at selected q, respectively. Figure 2(c) illustrates the corresponding large-q dispersion along $\bar{\Gamma}\bar{K}$. We note from Fig. 2 that the π plasmon disperses from ∼4 eV ($q \rightarrow 0$) to ∼12 eV ($q \sim 1.5$ Å^{-1}) along both $\bar{\Gamma}\bar{M}$ and $\bar{\Gamma}\bar{K}$ with an accompanying broadening of the peak, as expected. The dispersion of the $\pi + \sigma$ plasmon from ∼13 eV ($q \rightarrow 0$) to ∼30 eV ($q \sim 1.5$ Å^{-1}) can also be resolved. Intriguingly, the π-plasmon dispersion along $\bar{\Gamma}\bar{M}$ is accompanied by a low-energy, dispersive shoulder for q larger than 0.5 Å^{-1}, while such a phenomenon is absent along $\bar{\Gamma}\bar{K}$. We will come back to this feature and also the dispersion of the $\pi + \sigma$ plasmon later, and we now focus on the π-plasmon dispersion outlined in Fig. 3.
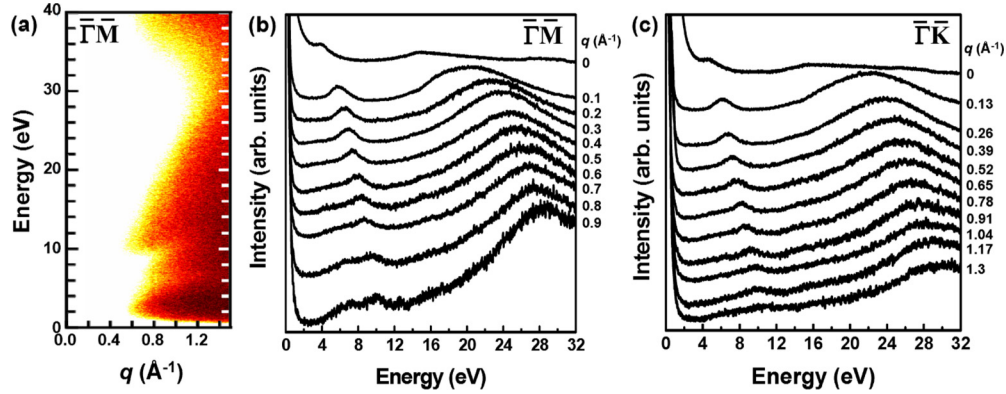
FIG. 2. (Color online) (a) The q-dependent EELS map toward the BZ boundary of graphene along $\bar{\Gamma}\bar{M}$. (b) The EELS spectra acquired at the selected q. (c) The q-dependent EELS spectra toward the BZ boundary along $\bar{\Gamma}\bar{K}$. The spectra in (b) and (c) were all normalized to the spectral intensity at ∼4.5 eV and then displaced vertically to improve the readability.

In Fig. 3(a), the experimental dispersions of the π plasmon along ΓQ and ΓP of parent graphite (the counterparts of $\bar{\Gamma}\bar{M}$ and $\bar{\Gamma}\bar{K}$, respectively) are also shown, and both exhibit the characteristic parabolic dependence ($\propto q^2$) [20–22]. In addition, the dispersions along the two in-plane directions are indistinguishable in the q range of $0-0.5\,\text{Å}^{-1}$ and start

FIG. 3. (Color online) (a) The π-plasmon dispersions in graphene along $\bar{\Gamma}\bar{M}$ (black squares) and $\bar{\Gamma}\bar{K}$ (red solid circles) and those in parent graphite along the ΓQ (gray open diamonds) and ΓP (red open circles) counterparts. The rescaling of the (b) π- and (c) $\pi + \sigma$-plasmon dispersions along $\bar{\Gamma}\bar{M}$ (black squares) and $\bar{\Gamma}\bar{K}$ (red circles) as a function of the $\sqrt{q}$ relation. The dashed gray line is a guide for the eyes for the linear $\sqrt{q}$ scaling toward the long-wavelength limit in (b) and throughout the q range in (c).

to deviate from each other at q above $0.5\,\text{Å}^{-1}$. In graphene [Fig. 3(a)], it is obvious that, near the long-wavelength limit ($0-0.5\,\text{Å}^{-1}$), the π-plasmon dispersions along $\bar{\Gamma}\bar{M}$ and $\bar{\Gamma}\bar{K}$ are neither quadratic as bulk graphite is nor linear as previously reported [17–19,23], although the dispersions tend to mimic those of parent graphite for q larger than $0.5\,\text{Å}^{-1}$. A nonlinear feature of the π-plasmon dispersions of graphene is indeed resolved in the q range of $0-0.5\,\text{Å}^{-1}$ [Fig. 3(a)], and the associated dispersions along $\bar{\Gamma}\bar{M}$ and $\bar{\Gamma}\bar{K}$ are almost the same. Now, we rescale the π-plasmon excitation energy as a function of $\sqrt{q}$ in Fig. 3(b). Notably, the nonlinear π-plasmon dispersion with q smaller than $0.5\,\text{Å}^{-1}$ is faithfully underlined by this $\sqrt{q}$ dependence [Fig. 3(b)], indicative of plasmons with a 2D character [3,6–9]. In principle, a perfectly 2D excitation should be further supported by the absence of out-of-plane electronic components of the state [4]. We carefully examined this possibility by tilting the graphene specimen (Fig. 4), a technique that has been exploited to reveal the anisotropic in-plane and out-of-plane signatures of the π and $\pi + \sigma$ plasmons in 3D parent graphite [20,30].
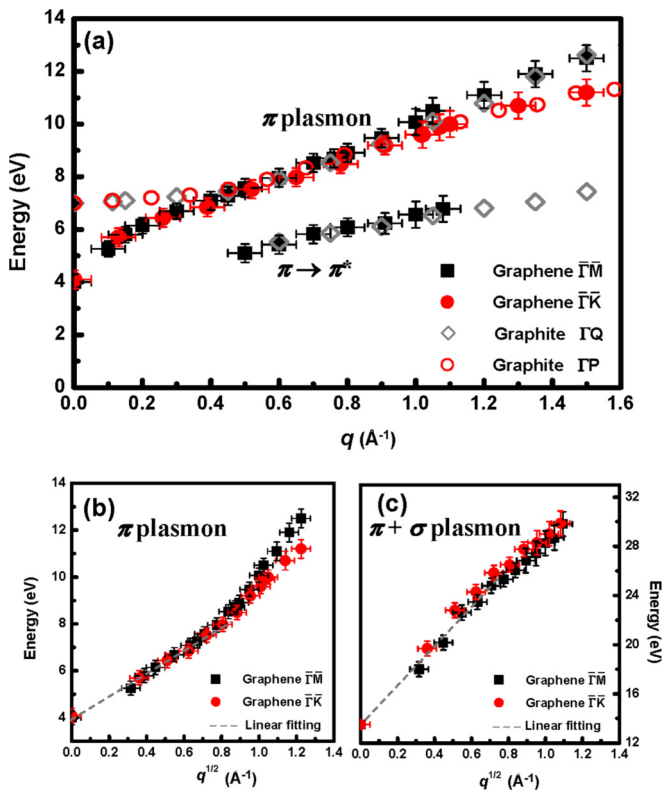
At first glance, the π-plasmon dispersion curves acquired for three separate tilting angles ($\alpha = 0°, 45°,$ and $60°$) in Fig. 4(a) are visibly different, showing a decrease in excitation energies with increasing α and therefore seemingly suggesting the existence of an out-of-plane factor such as parent graphite. Nevertheless, it should be noted from the inelastic scattering kinematics [inset in Fig. 4(a)] that, upon tilting, the effective momentum transfer is the q component projected onto the graphene sample q_s ($\approx q \cos\alpha$), rather than the primitive q. A rescaling of Fig. 4(a) as a function of q_s, shown in Fig. 4(b), reveals not only the profound equivalence of the three dispersion curves but, more importantly, the absence of any out-of-plane dispersive contribution to the π plasmon [4]. The 2D character of the π plasmon of graphene is now established. Although the $\pi + \sigma$ plasmon is too broad for such a sample-tilting inspection, a detailed examination of Fig. 3(c) indicates that the $\pi + \sigma$-plasmon dispersion basically scales with the $\sqrt{q}$ relation like the π plasmon and also reflects its 2D character.

With all these EELS elaborations in Figs. 2 –4, both the π and $\pi + \sigma$ plasmons of graphene clearly have a 2D essence.
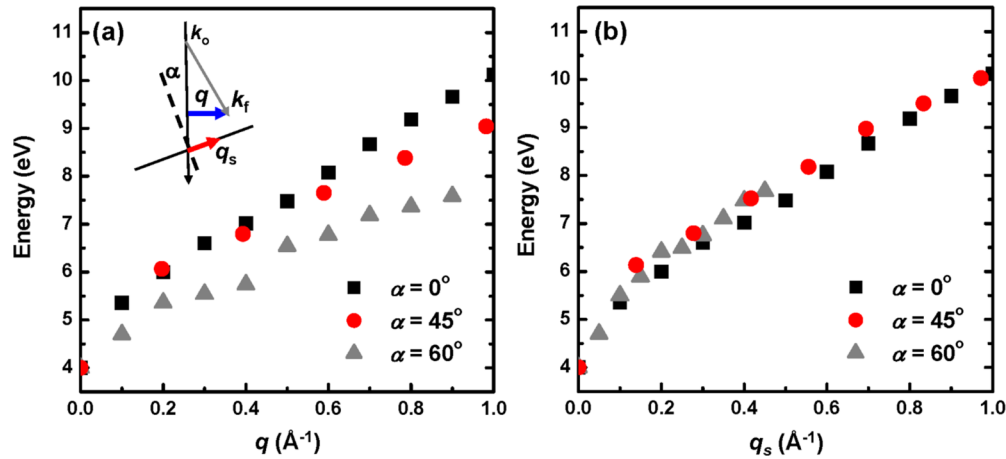
FIG. 4. (Color online) (a) The π-plasmon dispersions along $\bar{\Gamma}\bar{M}$ as a function of the tilting angle α of the graphene specimen from the normal incidence, with $\alpha = 0$ (black squares), 45° (red circles), and 60° (gray triangles). The inset shows the inelastic scattering kinematics at a given sample tilting of α. k_0, incident beam; k_f, inelastically scattered beam; q (blue), the momentum transfer corresponding to the inelastic scattering; q_s (red, $\approx q\cos\alpha$), the exact momentum transfer on the graphene sheet. (b) The rescaled dispersion curves as a function of q_s.

Previous reports of a linearly dispersed π plasmon should be a consequence of the limited q resolution therein [17–19]. It is also noted that a recent theoretical report on the collective excitations in graphene suggested a quadratic dispersion of the $\pi + \sigma$ plasmon [23], which is not found at all in our EELS investigations in Fig. 3(c). Moreover, in Fig. 2 we also did not observe the splitting of the $\pi + \sigma$ plasmon with a magnitude of a few eV for q larger than $\sim 1.0\,\text{\AA}^{-1}$ only along $\bar{\Gamma}\bar{K}$ that was reported in a recent EELS study of the plasmon dispersions of graphene (Ref. [17]). A splitting of this magnitude should be easily resolvable with our energy resolution of ~ 0.6 eV if it exists. This $\pi + \sigma$-plasmon splitting issue requires further investigation.

Having established the 2D character of the π and $\pi + \sigma$ plasmons of graphene, we now tackle the dispersive low-energy shoulder accompanying the π plasmon, which shows up only along $\bar{\Gamma}\bar{M}$ for q larger than $0.5\,\text{\AA}^{-1}$ and apparently further broadens the π-plasmon peaks [Figs. 2(b) and 3(a)]. Indeed, the same EELS feature was also reported in Ref. [17] and was qualitatively suggested to be a π-plasmon splitting, although its physical origin was not addressed. In the relevant theoretical work of Ref. [23], a similar splitting along $\bar{\Gamma}\bar{M}$ was found to disperse throughout the q range, unlike in the experimental observations in Figs. 2(b) and 3(a) and Ref. [17]. In Ref. [23], the dispersive shoulder was understood to be the π-plasmon splitting, but further details were not given. The splitting of a surface plasmon, which commonly occurs due to the electromagnetic coupling between two adjacent surfaces, is not expected to happen in single-layer graphene [31]. Therefore, we attempted to address the electronic origin of this low-energy shoulder along $\bar{\Gamma}\bar{M}$, and a close examination of Figs. 3(a) and 3(b) reveals three interesting characteristics. First, the same dispersive shoulder appears in parent graphite along ΓQ for q larger than $\sim 0.5\,\text{\AA}^{-1}$ [Fig. 3(a), open diamonds]. Second, the π-plasmon dispersions of graphite and graphene are basically identical in the q regime above $0.5\,\text{\AA}^{-1}$ [Fig. 3(a)], with the π-plasmon dispersion along ΓQ ($\bar{\Gamma}\bar{M}$) lying above that along ΓP ($\bar{\Gamma}\bar{K}$) in graphite (graphene).

Third, the scaling of the π-plasmon dispersions along $\bar{\Gamma}\bar{M}$ and $\bar{\Gamma}\bar{K}$ deviates from the $\sqrt{q}$ relation when q becomes larger than $0.5\,\text{\AA}^{-1}$ [Fig. 3(b)].

In parent graphite, the low-energy dispersive shoulder arises from a direct, nonvertical $\pi \to \pi^*$ interband transition present along ΓQ at large q and plays the role of blueshifting the associated π plasmon accordingly [20–22]. This thus-shifted π plasmon then sits on top of the dispersion curve along ΓP, as observed in Fig. 3(a), indicating an in-plane electronic anisotropy originating from the different characteristic band structures along the two inequivalent ΓQ and ΓP directions [20–22]. Indeed, the two in-plane counterpart directions of graphene, $\bar{\Gamma}\bar{M}$ and $\bar{\Gamma}\bar{K}$, are also intrinsically inequivalent. If we ignore the linearly dispersed Dirac cones at the $\bar{K}$ point, the band structures of graphene and graphite are otherwise similar [2,13,32]. For instance, the $\pi \to \pi^*$ interband transition of graphene also occurs at ~ 4 eV at the $\bar{M}$ point [2,13,15,32], and the corresponding band dispersion closely resembles that of graphite [32]. The low-energy dispersive feature along $\bar{\Gamma}\bar{M}$ could then be associated with a direct, nonvertical interband transition like the one in graphite, as confirmed by our *ab initio* calculations of the q-dependent electronic excitations in graphene and graphite within both RPA and ALDA (Fig. 5).

Figures 5(a) and 5(b) show the calculated q-dependent EELS spectra of graphite along ΓQ and ΓP, respectively, and Figs. 5(c) and 5(d) exhibit the readily derived π-plasmon dispersions and the low-energy dispersive feature. The experimental EELS results of graphite in Fig. 3(a) are also incorporated into Figs. 5(c) and 5(d) for comparison. Indeed, both the parabolic π-plasmon dispersion of graphite and the direct, nonvertical $\pi \to \pi^*$ transition along ΓQ at large q are nicely captured in our calculations [Figs. 5(c) and 5(d)]. In Figs. 5(e) and 5(f), the graphene-counterpart calculations are also notably consistent with the corresponding EELS observations of the $\sqrt{q}$ scaling of the π-plasmon dispersion and the onset of the low-energy dispersive transition at $q \sim 0.5\,\text{\AA}^{-1}$. For $q < 0.5\,\text{\AA}^{-1}$, where the π-plasmon excitation is dominant,
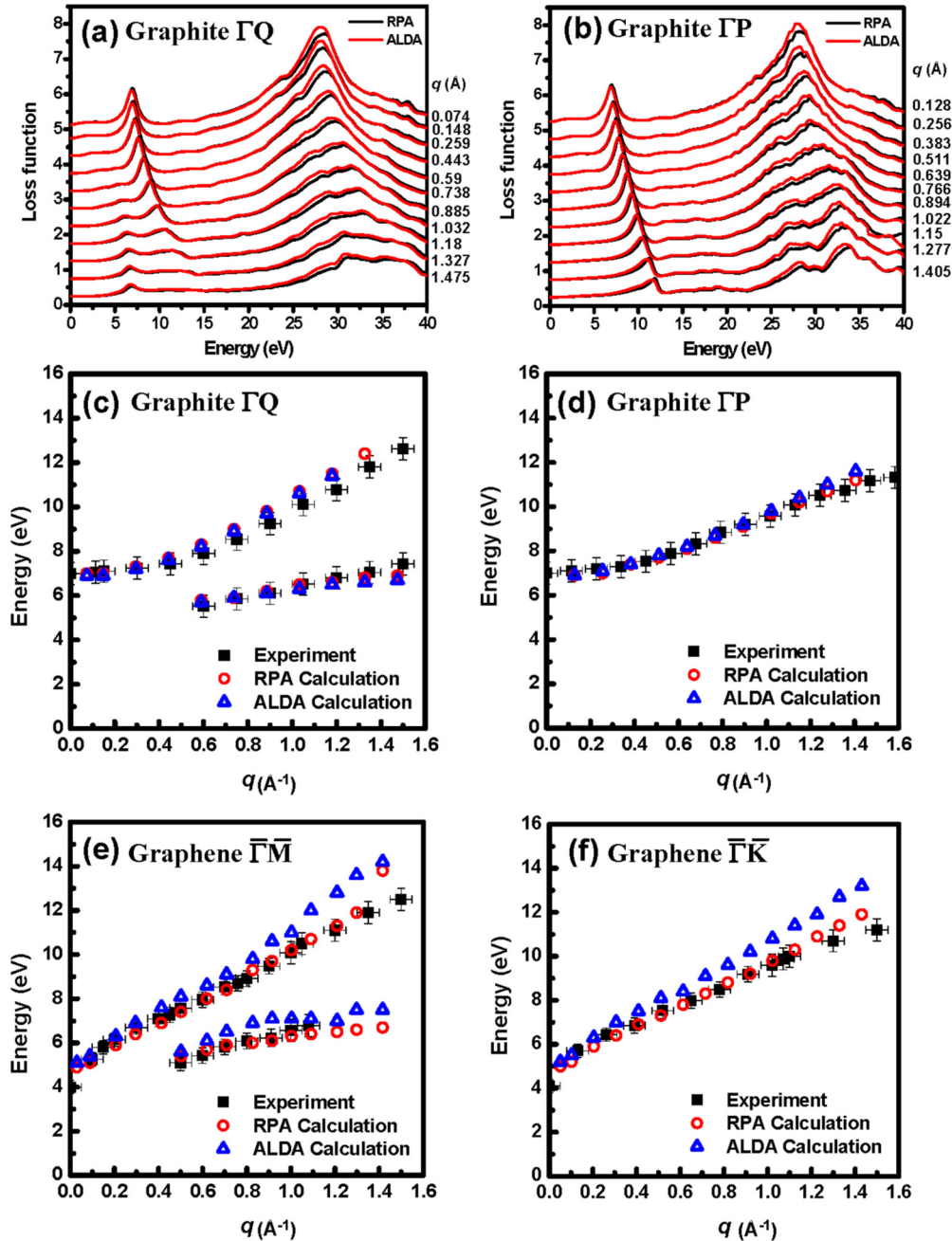
FIG. 5. (Color online) The calculated q-dependent EELS spectra of parent graphite along (a) ΓQ and (b) ΓP within the *ab initio* RPA (black) and ALDA (red) frameworks. (c) and (d) The dispersion curves derived from (a) and (b) along ΓQ and ΓP, respectively. The experimental EELS results in Fig. 3(a) are also shown for comparison (black squares). The calculated π-plasmon dispersions in graphene along (e) $\bar{\Gamma}\bar{M}$ and (f) $\bar{\Gamma}\bar{K}$ within the *ab initio* RPA (red open circles) and ALDA (blue open triangles) methods and also the associated EELS experiments in Fig. 3(a) (black squares).

the electronic screening effect is strong due to the large real part of the complex dielectric function ($\varepsilon = \varepsilon_1 + i\varepsilon_2$), as shown in the corresponding calculations in Fig. 6(a), and the intensity of the low-energy interband transition features is readily overwhelmed by the plasmon (see the associated loss function), becoming invisible in EELS. For $q > 0.5\,\text{Å}^{-1}$, the π-plasmon oscillation is, however, increasingly damped with a diminishing intensity, and the lower-energy peak due to the interband transition can then emerge as a shoulder [see the calculated loss function, Fig. 6(b)].

Nonetheless, there exists a systematic overestimation for the ALDA results compared with the RPA calculations of graphene [Figs. 5(e) and 5(f)]. Indeed, the ALDA method is optimal for 3D matters with a nearly homogeneous electron density, and the previous ALDA calculations of such a material, Al, have been found to satisfactorily depict the characteristic plasmon dispersion [33]. By contrast, graphene is purely 2D, and the associated electron density changes abruptly along the out-of-plane direction; thus, a 2D system is not an ideal geometry for ALDA. For the ALDA method to be more
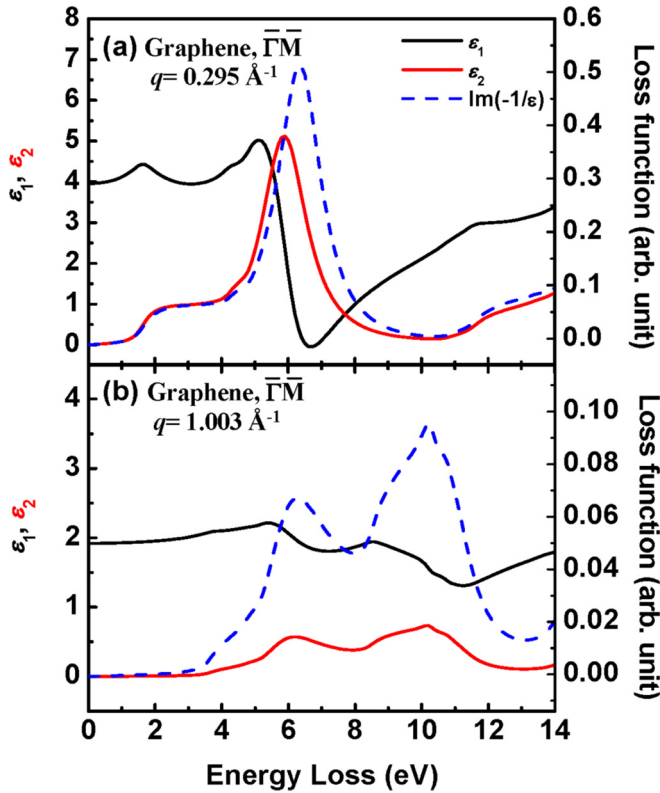
FIG. 6. (Color online) The q-dependent complex dielectric function, $\varepsilon = \varepsilon_1 + i\varepsilon_2$, and the thus-derived electron-energy loss function, $\mathrm{Im}(-1/\varepsilon)$, of graphene along $\bar{\Gamma}\bar{M}$ for (a) $q = 0.295\,\text{Å}^{-1}$ and (b) $q = 1.003\,\text{Å}^{-1}$ from the RPA calculations.

appropriate for 2D systems, an improved exchange-correlation potential would be required, which is an intriguing challenge to be resolved in the future. Otherwise, the general agreement between the theoretical calculations and experiments in Fig. 5 points to a close electronic similarity between 2D graphene and 3D graphite for q larger than $0.5\,\text{Å}^{-1}$ as a result of the close resemblance of their electronic structures [32]. This electronic similarity underlines the three features of Figs. 3(a) and 3(b) as a whole and, more importantly, establishes the in-plane electronic anisotropy of graphene just like in the parent graphite.

So far, we have investigated the electronic excitations of graphene above $\sim$4 eV. We intend to further compare the π plasmon to the 2D Dirac plasmon at 0–1 eV [3,7,8]. In previous π-plasmon studies of graphene [17,18,23], the reported linear dispersion, proven to be incorrect herein, was correlated with transitions from the linearly dispersed Dirac cones [18] and became a generally accepted notion [17,23]. The possibility for the Dirac fermions to entangle with the π plasmon is vanishingly small since the spectral weight of carriers in the Dirac cones centers below $\sim$1 eV due to its small carrier density ($\sim 10^{13}\,\text{cm}^{-2}$) [7,8,10–12], which is two orders of magnitude below that of π valence electrons, as discussed later. The correlation of the reported linear dispersion of the π plasmon to the linear Dirac cones can be safely discounted. Nonetheless, the π-plasmon onset at $\sim$4 eV as $q \to 0$ [Fig. 3(a)] coincides with the $\pi \to \pi^*$ vertical

interband transition of $\sim$4 eV at the $\bar{M}$ point [15,32]. This raises the possibility of mixed collective and single-particle essences for the π plasmon [19], and an electromagnetic oscillation of this type, the so-called plexciton (coupling of interband transitions and plasmon oscillators), has been reported [8,34].

The continuous π-plasmon dispersion from $\sim$4 eV ($q \to 0$) to $\sim$12 eV ($q \sim 1.5\,\text{Å}^{-1}$) and its $\sqrt{q}$ scaling in Fig. 3(b) follow the equation $\omega_p(q) = \beta + \sqrt{\gamma q}$, derived for a 2D collective excitation due to an interband transition, with ω_p being the dispersive plasmon energy, β being the single-particle oscillator strength, and $\gamma = \sqrt{2\pi n_{2D}e^2/m\varepsilon}$ [6,9]. It should be noted that the derivation of γ has been based on the long-range Coulomb response of a noninteracting 2DEG to an external longitudinal electric field [6,9], analogous to the longitudinal excitations in our EELS [31], where n_{2D} is the 2D electron density (in cm^{-2}), e is the elementary charge, m is the effective mass of electron ($0.06m_0 - 0.07m_0$, with m_0 being the rest mass of an electron) [13,14], and ε is the dielectric constant (set to unity, for convenience). The square root of γ was determined to be $\sim$5.18 from Fig. 3(b), and the dispersion relation of the π plasmon can now be written as $\omega_P \approx 4 + 5.18\sqrt{q}$ for q smaller than $0.5\,\text{Å}^{-1}$. We were then able to obtain the corresponding 2D π-electron density as $\sim 2 \times 10^{15}\,\text{cm}^{-2}$, which is notably on the same order as the total π electrons integrated in the first BZ of graphene, $\sim 3.8 \times 10^{15}\,\text{cm}^{-2}$ ($\approx 4/\sqrt{3}a^2$) [14]. A difference in the π-electron densities by a factor of 2 can be noted, implying that, in the case of the noninteracting 2DEG model [6,9], only about half of the total π electrons participate in the corresponding 2D plasmon excitation, with the rest of the oscillator strength being taken up by the single-particle interband transition at nearly the same energy as the π plasmon. Hence, the agreement between the two evaluated electron densities can be a reasonable one, and the consistency between the thus-deduced single-particle oscillator strength β of $\sim$4 eV and the associated interband transition ($\sim$4 eV) is satisfactory, suggesting a single-particle mixture for the collective 2D π plasmon. Indeed, such a suggestion was also raised recently on the basis of the proposal that the linear dispersion of the π plasmon observed could be entangled with a linearly dispersed $\pi \to \pi^*$ interband transition at lower energy along $\bar{\Gamma}\bar{M}$ at $q \leqslant 0.5\,\text{Å}^{-1}$ [19]. Although we have firmly established the $\sqrt{q}$ dispersion of the π plasmon at $q \leqslant 0.5\,\text{Å}^{-1}$ and the onset of the $\pi \to \pi^*$ transition only above $0.5\,\text{Å}^{-1}$ for q along $\bar{\Gamma}\bar{M}$, this coincidence in the suggestion is still intriguing. Nevertheless, we are conservative about further terming the π plasmon of graphene as a plexciton, which features a coherent coupling between the single-particle and collective oscillator strengths [34]. The broad π plasmon observed herein [Figs. 2(b) and 2(c)] does not seem to support this element of coherent coupling.

IV. CONCLUSION

Using q-dependent EELS, we have revealed the 2D essence of the π and $\pi + \sigma$ plasmons of graphene with the convincing observation of a characteristic $\sqrt{q}$ dispersion of 2D collective excitations near the long-wavelength limit. For the π plasmon, evidence for the absence of any dispersive component along

the out-of-plane direction, which is a further signature of a 2D excitation, was also presented. In addition, a low-energy, dispersive shoulder accompanied by the π-plasmon dispersion along $\bar{\Gamma}\bar{M}$, but not along the other principal vector of $\bar{\Gamma}\bar{K}$ in the ab plane, was theoretically tackled and was found to arise from a direct, nonvertical interband transition along only $\bar{\Gamma}\bar{M}$, revealing an in-plane electronic anisotropy. The quantitative evaluation of the $\sqrt{q}$ scaling of the π plasmon microscopically reveals that this 2D collective oscillation is also electronically intermingled with the single-particle

$\pi \rightarrow \pi^*$ interband transition, which is totally different from the well-known 2D Dirac plasmon of graphene with a purely Dirac fermion contribution.

[1] A. K. Geim and K. S. Novoselov, Nat. Mater. **6**, 183 (2007).

[2] A. H. Castro Neto, F. Guinea, N. M. R. Peres, K. S. Novoselov, and A. K. Geim, Rev. Mod. Phys. **81**, 109 (2009).

[3] S. Das Sarma and E. H. Hwang, Phys. Rev. Lett. **102**, 206412 (2009).

[4] M. Bianchi, D. Guan, S. Bao, J. Might, B. B. Iversen, P. D. C. King, and P. Hofmann, Nat. Commun. **1**, 128 (2010).

[5] Y.-C. Lin, D. O. Dumcenco, Y.-S. Huang, and K. Suenaga, Nat. Nanotechnol. **9**, 391 (2014).

[6] A. Nagashima, K. Nuka, H. Itoh, T. Ichinokawa, C. Oshima, S. Otani, and Y. Ishizawa, Solid State Commun. **83**, 581 (1992).

[7] Y. Liu, R. F. Willis, K. V. Emtsev, and Th. Seyller, Phys. Rev. B **78**, 201403 (2008).

[8] C. Tegenkamp, H. Pfnür, T. Langer, J. Baringhaus, and H. W. Schumacher, J. Phys. Condens. Matter **23**, 012001 (2011).

[9] F. Stern, Phys. Rev. Lett. **18**, 546 (1967).

[10] J. A. Gerber, S. Berweger, B. T. O'Callahan, and M. B. Raschke, Phys. Rev. Lett. **113**, 055502 (2014).

[11] P. Alonso-González, A. Y. Nikitin, F. Golmar, A. Centeno, A. Pesquera, S. Vélez, J. Chen, G. Navickaite, F. Koppens, A. Zurutuza, F. Casanova, L. E. Hueso, and R. Hillenbrand, Science **344**, 1369 (2014).

[12] X. Luo, T. Qiu, W. Lu, and Z. Ni, Mater. Sci. Eng. R **74**, 351 (2013).

[13] S. Y. Zhou, G.-H. Gweon, J. Graf, A. V. Fedorov, C. D. Spataru, R. D. Diehl, Y. Kopelevich, D.-H. Lee, S. G. Louie, and A. Lanzara, Nat. Phys. **2**, 595 (2006).

[14] P. R. Wallace, Phys. Rev. **71**, 622 (1947).

[15] T. Eberlein, U. Bangert, R. R. Nair, R. Jones, M. Gass, A. L. Bleloch, K. S. Novoselov, A. Geim, and P. R. Briddon, Phys. Rev. B **77**, 233406 (2008).

[16] C. Kramberger, R. Hambach, C. Giorgetti, M. H. Rümmeli, M. Knupfer, J. Fink, B. Büchner, L. Reining, E. Einarsson, S. Maruyama, F. Sottile, K. Hannewald, V. Olevano, A. G. Marinopoulos, and T. Pichler, Phys. Rev. Lett. **100**, 196803 (2008).

[17] P. Wachsmuth, R. Hambach, M. K. Kinyanjui, M. Guzzo, G. Benner, and U. Kaiser, Phys. Rev. B **88**, 075433 (2013).

[18] J. Lu, K. P. Loh, H. Huang, W. Chen, and A. T. S. Wee, Phys. Rev. B **80**, 113410 (2009).

[19] M. K. Kinyanjui, C. Kramberger, T. Pichler, J. C. Meyer, P. Wachsmuth, G. Benner, and U. Kaiser, Europhys. Lett. **97**, 57005 (2012).

[20] K. Zeppenfeld, Z. Phys. **243**, 229 (1971).

[21] H. Venghaus, Phys. Status Solidi B **66**, 145 (1974).

[22] U. Büchner, Phys. Status Solidi B **81**, 227 (1977).

[23] V. Despoja, D. Novko, K. Dekanić, M. Šunjić, and L. Marušić, Phys. Rev. B **87**, 075447 (2013).

[24] P. A. Midgley, Ultramicroscopy **76**, 91 (1999).

[25] J. C. Mayer, A. K. Geim, M. I. Katsnelson, K. S. Novoselov, T. J. Booth, and S. Roth, Nature (London) **446**, 60 (2007).

[26] J. P. Perdew and A. Zunger, Phys. Rev. B **23**, 5048 (1981).

[27] J. Yan, J. J. Mortensen, K. W. Jacobsen, and K. S. Thygesen, Phys. Rev. B **83**, 245122 (2011).

[28] J. J. Mortensen, L. B. Hansen, and K. W. Jacobsen, Phys. Rev. B **71**, 035109 (2005).

[29] W. J. Enkovaara et al., J. Phys. Condens. Matter **22**, 253202 (2010).

[30] C. H. Chen and J. Silcox, Phys. Rev. Lett. **35**, 390 (1975).

[31] H. Raether, Excitation of Plasmons and Interband Transitions by Electrons, Springer Tracts in Modern Physics Vol. 88 (Springer, Berlin, 1980).

[32] A. G. Marinopoulos, L. Reining, A. Rubio, and V. Olevano, Phys. Rev. B **69**, 245419 (2004).

[33] A. A. Quong and A. G. Eguiluz, Phys. Rev. Lett. **70**, 3955 (1993).

[34] N. T. Fofang, T.-H. Park, O. Neumann, N. A. Mirin, P. Nordlander, and N. J. Halas, Nano Lett. **8**, 3481 (2008).